*Proceedings of the*
*Annual Stability Conference*
*Structural Stability Research Council*
*Louisville, Kentucky, April 13-16, 2021*

# Stability of stainless steel frames with different beam-to-column connection types

Mohammed M. Eladly[1], Benjamin W. Schafer[2]

## Abstract

Despite the considerable impact of end conditions on the stability of beams, only a small proportion of investigations into the lateral-torsional buckling (LTB) behavior of stainless steel beams have considered cases with actual end conditions. The current paper presents a numerical study on the effect of beam-to-column connection type on the stability of frame beams produced from stainless steel. Several connection types were examined, including extended end-plate, flush end-plate, and shear end-plate connections. The study was carried out using a verified finite element model that carefully takes into account the complex interactions between connection components. The results demonstrated that the critical moment for lateral-torsional buckling of the beam is obviously affected by the type of beam-to-column joints. While beams with stiffened extended end-plate (SEEP) connections had the greatest critical moment among the investigated cases, beams with shear end-plate connections showed the lowest capacity (50% of that of SEEP joints). Finally, based on FE data, a modification to the analytically-predicted critical moments, using a factor accounting for end connection stiffness, is proposed.

## 1. Introduction

Over the past few decades, stainless steel has attracted the attention of many researchers in the structural engineering field (e.g., Baddoo 2008, Gardner 2005, Gedge 2008, Rossi 2014). Stainless steel may be beneficially employed in structures located in coastal zones, or in buildings in corrosive urban or industrial environments, owing to its excellent corrosion resistance. Additionally, when employed for elements requiring high levels of ductility, e.g. due to blast, progressive collapse, or seismic demands, stainless steel may provide a unique solution (Di Sarno et al. 2003, Di Sarno et al. 2006, Zhou et al. 2016). Due to the relatively high initial cost of stainless steel, efficient design of structural elements is required. This, for large sections, often results in design of slender members with their associated stability challenges.

[1] Graduate Research Assistant, Department of Civil and Systems Engineering, Johns Hopkins University, <eladly@jhu.edu>
[2] Professor, Department of Civil and Systems Engineering, Johns Hopkins University, <schafer@jhu.edu>

Most international design codes for stainless steel structures provide rules that are originally developed for carbon steel with limited modifications. These modifications may not sufficiently account for the material response of stainless steel which is evidently different from that of ordinary carbon steel, particularly when instability takes place and the material nonlinearity exerts influence on the response.

Lateral-torsional buckling (LTB) (an instability phenomenon which combines both minor axis bending and torsion) governs the structural response of most laterally un- or partially-restrained beams. Many of the studies in this area (Bailey et al. 1996, Kala 2015, Kucukler el al. 2015, Vila Real et al. 2003) are focused on carbon steel beams, while a limited number of investigations considered LTB of beams produced from stainless steel (Anwar-Us-Saadat et al. 2018, Fortan et al. 2021, Sorf et al. 2020, Vila Real et al. 2008, Wong et al. 2015). Moreover, the majority of the latter studies (investigating the stability of stainless steel beams) did not consider the effect of actual beam end-conditions, assuming the so-called ‘‘fork boundary conditions’’ at the beam ends.

In this paper, the influence of real end-conditions on the stability of stainless steel frame beams is investigated. First, a finite element (FE) model for performing linear LTB analysis is described and verified against different analytical methods reported in international structural design standards. Subsequently, the numerical model was exploited to perform a parametric study on the LTB behavior of beams with different end-conditions, including standard fork conditions in addition to extended end-plate, flush end-plate, and shear end-plate beam-to-column connections. Finally, a modification factor accounting for end connection stiffness was suggested based on the generated FE data. The provided studies investigate only the idealized elastic buckling response, and are thus applicable to both carbon and stainless steel, work to investigate the complete material and geometric nonlinear response for stainless steel is planned.

## 2. Finite element modeling

FE models of stainless steel beam-to-column connections have been previously developed by the first author (Eladly 2020a, Eladly 2020b). The present numerical study on LTB behavior of frame beams relies on this previous work, and is carried out using ABAQUS (ABAQUS 2012) with only slight modifications to perform the linear buckling analysis. A brief description of the adopted model is provided in the following, while a detailed description of the connection model may be found in Eladly (2020a).

A four-node shell element with reduced integration (S4R) was used for the beams, columns and connections’ parts. Based on a mesh sensitivity analysis performed using different mesh sizes, a fine mesh (4-7.5 mm element length on one side) was chosen for the connection parts adjacent to the joint region (e.g. end-plate, and column flange), while the other portions of the model, distant from the connection area, used a larger element size (20-30 mm), as shown in Fig. 1.

CARTESIAN connector elements (ABAQUS 2012) were used for modeling the stainless steel bolts. To prohibit local deformations that can occur at connectors’ nodes, “Rigid Body” constraints (ABAQUS User’s Manual 2012) were adopted, as displayed in Fig. 2. For the contact relationships between non-welded elements (e.g. between the column flange and shear end-plate), surface-to-surface contact comprising a “Hard” contact relationship with a “Coulomb friction” formulation

was employed. In order to represent the stainless steel material's response, the bi-stage Ramberg-Osgood model (Rasmussen 2003) was chosen. However, since the study here focuses on buckling response only the initial modulus is utilized at this stage. Future work examining full geometric and material nonlinear response is planned.

To solve the linear eigen-value problem involved in a linear buckling analysis, the subspace iteration method available in ABAQUS (also known as the inverse block power method in the applied mathematics literature) was used (Bathe 1998). For better visualization of the deformed shapes the "Render shell thickness" option (provided in ABAQUS CAE) is used in the remainder of the current paper (Fig. 3).

A thorough verification of the model's ability to capture the behavior of stainless steel bolted connections is reported in Eladly's numerical study (Eladly 2020a), while the validation of the model's capability to perform a linear lateral torsional buckling analysis is presented in the following section.

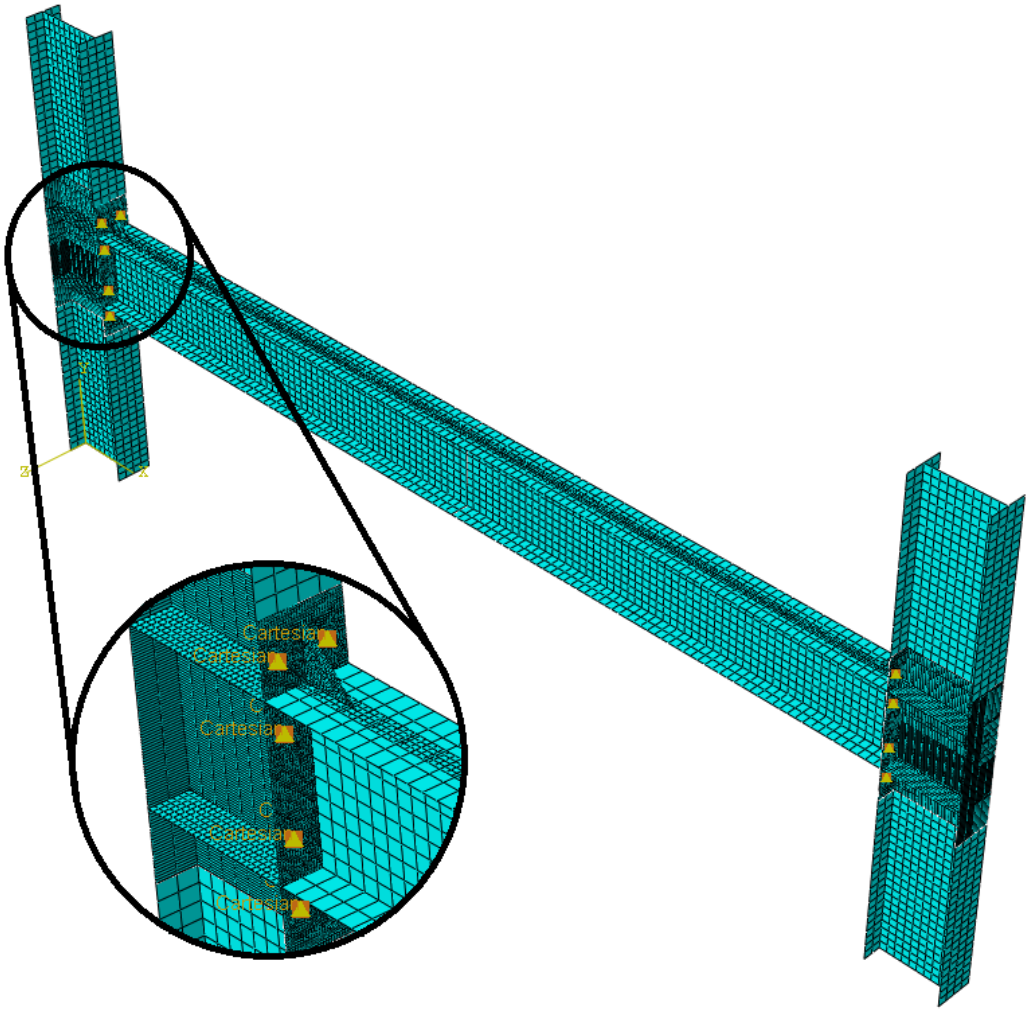

Figure 1: 3D shell FE model of a stainless steel beam connected to columns by extended end-plate joints

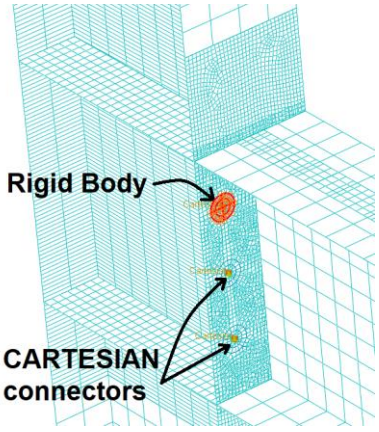


Figure 2: Stainless steel bolts represented by CARTESIAN elements in a 3D shell model of a flush end-plate connection

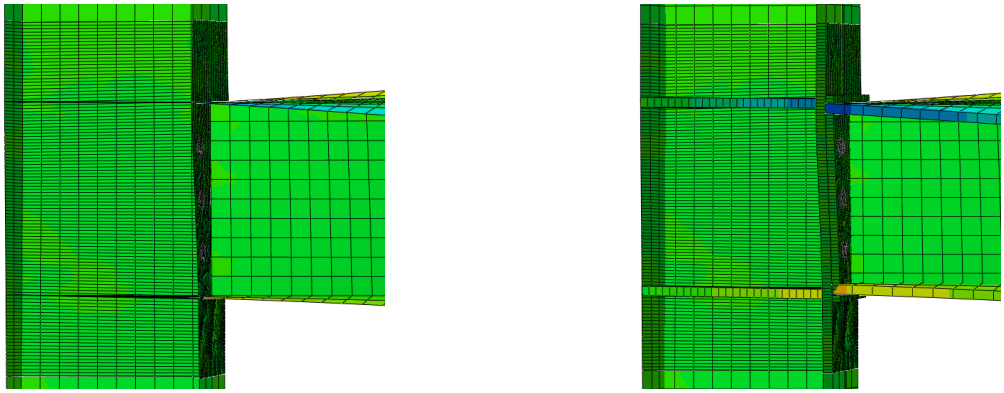

(a) without utilizing "Render shell thickness" option (b) utilizing "Render shell thickness" option (used in the remainder of this paper)

Figure 3: Comparison of the deformed shapes of a flush end-plate connection (modelled by a 3D shell model) with and without utilizing "Render shell thickness" option

## 3. Verification of the finite element model

In this section, the suggested FE model accuracy in carrying out an eigenvalue buckling analysis of stainless steel beams is verified against analytical models found in the literature. Three different analytical models were considered including Nethercot and Rockey (Nethercot and Rockey 1972), ANSI/AISC 360-10 (AISC 2010b), and SSRC Guide (Ziemian 2010). Additionally, the predictions of LTBeam (Galéa 2003), a finite element software specially developed for providing the solution for the elastic critical moment of beams with arbitrary cross-section and non-uniform geometry, are included in the verification.

All the critical elastic moment predictions of these analytical methods are similar in the case of an unbraced beam with a doubly-symmetric cross section subjected to a uniform moment, and having ends that are laterally and torsionally pinned. The moment in such a case (abbreviated to $M_{0cr}$) can be approximated using the following equation (Timoshenko 1936):

$$M_{0cr} = \frac{\pi}{L}\sqrt{EI_yGJ + \left(\frac{\pi E}{L}\right)^2 I_y C_w} \quad (1)$$

where L is the laterally unsupported length, E is the Young's modulus, $I_y$ is the minor-axis second moment of area, G is the shear modulus, J is the St. Venant torsional constant, and $C_w$ is the warping torsional constant. This critical moment may be multiplied by an equivalent uniform moment factor, $C_b$ (AISC 2010a), to take into consideration the impact of a moment gradient either from unequal end moments or transverse loading imposed between laterally braced ends at the beam's shear center level, hence:

$$M_{cr} = \frac{C_b \pi}{L} \sqrt{E I_y G J + \left(\frac{\pi E}{L}\right)^2 I_y C_w} \tag{2}$$

To account for the load height effect, which greatly influences the critical moment, some methods propose the application of an effective length factor to the unsupported member length, whilst others instead offer either a global coefficient multiplier to Eq. 1, or use another method to consider the increased demand resulting from top-flange loading. In the next subsections, three methods considering the load height impact are briefly presented, then their results are compared with those numerically-predicted.

*3.1 Nethercot and Rockey (abbreviated to NR)*

Nethercot and Rockey (1972) suggested expressions for a modification factor (α) to Eq. 1 to take into consideration the impact of different end restraint and loading conditions. Three particular load heights are accounted by the proposed equations:

$$\begin{gathered} \alpha = AB \text{ for bottom-flange loading} \\ \alpha = A \text{ for shear-centre loading} \\ \alpha = A/B \text{ for top-flange loading} \end{gathered} \tag{3}$$

Table 1 lists the suggested parameters A and B for two common transversely-loaded cases: a mid-span point load, and a uniformly-distributed load. The parameter A is similar to the equivalent uniform moment factor ($C_b$), while the parameter B considers the load height effect. The torsional parameter R can be determined by the following equation:

$$R = L \sqrt{\frac{GJ}{EC_w}} \tag{4}$$

*3.2 ANSI/AISC 360-10 (abbreviated to AISC)*

The commentary of AISC Specification (AISC 2010b) offers a method for considering the load height effect by adjusting the following equation that determines the critical lateral-torsional buckling for compact doubly-symmetric I-shaped beams:

$$M_{cr} = \frac{C_b \pi^2 E \sqrt{I_y C_w}}{L^2} \sqrt{1 + 0.078 \frac{JL^2}{h\sqrt{I_y C_w}}} \tag{5}$$

where h is the distance between the flange centroids.

The commentary adopts a conservative approximate approach to determine the decreased critical moment of such a beam under top-flange loading by setting the right-hand square root expression in Eq. 5 equal to unity resulting in Eq. 6:

$$M_{cr} = \frac{C_b \pi^2 E \sqrt{I_y C_w}}{L^2} \tag{6}$$

Table 1: Load height parameters for simply-supported beams (Nethercot and Rockey 1972)

| Load cases | A | B |
|---|---|---|
| Mid-span point load | 1.35 | $1 - \frac{1.779}{R^2} + \frac{2.039}{R}$ |
| Uniformly-distributed load | 1.123 | $1 - \frac{1.522}{R^2} + \frac{1.681}{R}$ |

*3.3 SSRC Guide (abbreviated to SSRC)*

To consider the load height impact, the SSRC Guide (Ziemian 2010) suggests a procedure that is analogous to that of Nethercot and Rockey (1972) except that it is proposed, depending on the study of Helwig et al. (1997), that parameter B can be specified equal to 1.4, with $C_b$ (as per AISC 2010a) used as parameter A. Helwig et al. (1997) found that for simply-supported beams under point load at mid-span or under a uniformly-distributed load, B is relatively independent on the parameter R, and a constant value of 1.4 provides acceptable and conservative predictions for all but short, stocky sections. The approach was extended to apply to any load height by replacing $C_b$ with $C_b^*$ as follows:

$$C_b^* = 1.4^{2y/h} C_b \leq 3.0 \tag{7}$$

where y is the vertical distance from mid-height of the cross section to the point of load application (positive when the load is below the shear center).

*3.4 Comparison of FE and analytical results*

To examine the predictions of the FE model, its results were compared against those predicted by the analytical methods described in Section 3.1-3.3 and with LTBeam (a finite element software adopting 14 DOF beam elements to solve LTB problems). The geometric and material properties of the beam used in the verification are listed in Table 2. In all considered cases, the beam was modeled fork conditions (supported against transverse displacement and rotation, but warping free) at both end sections. Several loading types: distributed uniform load, concentrated force at midspan, opposite and equal end moments; and points of load application: top flange, midheight, bottom flange, were taken into account. Moreover, in addition to the pinned (fork) end conditions fully fixed end conditions were also considered. As shown in Tables 3 and 4, nineteen different cases were investigated, of which thirteen have warping-free ends while the ends of the remaining cases were warping-prevented.

Tables 3 and 4 present a comparison of the critical moments for the nineteen investigated cases predicted by (i) the FE model suggested in this paper; (ii) the three analytical methods reported in Sections 3.1-3.3; and (iii) LTBeam software. Fig. 4 illustrates the FE critical mode shapes for beams with fork supports subjected to distributed load applied at the top flange. From the comparison, it is clear that there is a good agreement between the results of the shell FE model and

LTBeam in most cases. On the other hand, the agreement between the numerically- and analytically-predicted critical moments while excellent when the ends are pinned, has obvious discrepancies in the cases of fixed end restraints. This is expected because the utilized analytical methods were originally developed for beams with pinned end restraints and then modified to handle fixed ends. Hence, these models provide the greatest accuracy for the former end conditions, and less accurate results for the latter due to the involved approximations. It can also be noted that, in almost all cases, the values of $M_{cr}$ predicted by the FE model are comparable to the critical moments calculated by one or more of the other investigated methods.

Table 2: Geometric and material properties of the beam employed in the verification

| | |
|---|---|
| Buckling length (mm) | 3000 |
| Total height (mm) | 240 |
| Web thickness (mm) | 10 |
| Flange width (mm) | 120 |
| Flange thickness (mm) | 12 |
| Elastic modulus (N/mm$^2$) | 200000 |
| Poisson's ratio | 0.3 |

Based on the comparisons presented in Tables 3 and 4, it could be said that, in the cases of beams with warping-free pinned ends, SSRC and NR methods provide accurate predictions regardless of the point of load application, while AISC method accurately predicts the critical moment when the load is applied at midheight and conservatively estimates it in the case of top-flange loading. When the beams' ends are fixed, the predictions of the three investigated analytical methods are not always accurate; the errors in AISC predictions in some cases reached above 40%. A modification to AISC expressions for lateral torsional buckling capacity of beams is recommended.

## 4. Parametric study

There is a limited number of studies exploring the effect of beam-to-column connection type on the stability of stainless steel beams. Hence, as a first step towards studying LTB in stainless steel frameworks, the suggested numerical model (described and verified in Sections 2 and 3) was exploited to conduct a FE parametric study on the linear elastic lateral-torsional buckling behavior of stainless steel frame beams connected to columns using endplate joints. Several connection types were investigated in the study, including shear end-plate; flush end-plate; unstiffened extended end-plate; and stiffened extended end-plate beam-to-column joints. Additionally, for comparison purposes, beams with pinned and fixed fork end conditions were included in the study. The schematic outline of the beams with beam-to-column connection at their ends, and the details of the considered beam-to-column connection types are illustrated in Figs. 5 and 6.

The geometric and material parameters of the beam investigated in the parametric study can be found in Table 2. As shown in Fig. 5, the lower ends of columns are fixed, while the upper ends have restrained horizontal displacements. The thicknesses of endplate, column stiffeners, and rip stiffeners were 10 mm, 12 mm and 10 mm, respectively. Fully-threaded hand-tightened grade A80 M16 stainless steel bolts were employed to connect the endplate to the column flange in all the investigated connection types.

Table 3: Comparison of critical moments (in kN.m) predicted by the developed FE model and those calculated by different analytical and numerical methods (absolute values)

| ID | Loading | Point of load application | Support of both ends | Warping | FEM $C_b$ | FEM | AISC | SSRC | NR | LTBeam |
|---|---|---|---|---|---|---|---|---|---|---|
| DL-PS-TF-WF | Distributed uniform load | Top Flange | Pinned | Free | 0.81 | 116.15 | 98.71 | 120.94 | 120.27 | 118.33 |
| PL-PS-TF-WF | Concentrated force at midspan | Top Flange | Pinned | Free | 0.91 | 130.50 | 114.29 | 132.70 | 136.15 | 133.16 |
| EM-PS-MH-WF | Opposite and equal end moments | Midheight | Pinned | Free | 1.00 | 143.50 | 140.95 | 140.95 | 140.95 | 140.35 |
| DL-PS-MH-WF | Distributed uniform load | Midheight | Pinned | Free | 1.09 | 157.13 | 160.17 | 160.17 | 159.27 | 158.79 |
| PL-PS-MH-WF | Concentrated force at midspan | Midheight | Pinned | Free | 1.27 | 182.25 | 185.46 | 185.46 | 190.28 | 191.16 |
| DL-PS-BF-WF | Distributed uniform load | Bottom Flange | Pinned | Free | 1.44 | 207.00 | --- | 212.12 | 210.93 | 212.88 |
| PL-PS-BF-WF | Concentrated force at midspan | Bottom Flange | Pinned | Free | 1.84 | 264.38 | --- | 259.20 | 265.94 | 272.67 |
| PL-FS-TF-WF | Concentrated force at midspan | Top Flange | Fixed | Free | 0.82 | 118.28 | 167.04 | 193.94 | 182.59 | 104.66 |
| DL-FS-TF-WF | Distributed uniform load | Top Flange | Fixed | Free | 1.11 | 159.55 | 206.81 | 253.41 | 164.46 | 148.26 |
| PL-FS-MH-WF | Concentrated force at midspan | Midheight | Fixed | Free | 1.58 | 226.36 | 271.06 | 271.06 | 309.04 | 241.81 |
| DL-FS-MH-WF | Distributed uniform load | Midheight | Fixed | Free | 2.40 | 344.84 | 335.60 | 335.60 | 258.11 | 365.91 |
| PL-FS-BF-WF | Concentrated force at midspan | Bottom Flange | Fixed | Free | 3.52 | 505.76 | --- | 378.84 | 523.06 | 547.28 |
| DL-FS-BF-WF | Distributed uniform load | Bottom Flange | Fixed | Free | 4.88 | 699.67 | --- | 422.85 | 405.09 | 882.68 |
| PL-FS-TF-WP | Concentrated force at midspan | Top Flange | Fixed | Prevented | 1.39 | 199.69 | --- | --- | 304.56 | 213.05 |
| PL-FS-MH-WP | Concentrated force at midspan | Midheight | Fixed | Prevented | 2.31 | 331.13 | --- | --- | 437.62 | 433.90 |
| DL-FS-TF-WP | Distributed uniform load | Top Flange | Fixed | Prevented | 2.32 | 333.30 | --- | --- | 305.86 | 361.45 |
| DL-FS-MH-WP | Distributed uniform load | Midheight | Fixed | Prevented | 4.48 | 642.90 | --- | --- | 391.96 | 716.53 |
| PL-FS-BF-WP | Concentrated force at midspan | Bottom Flange | Fixed | Prevented | 5.28 | 757.35 | --- | --- | 628.82 | 861.97 |
| DL-FS-BF-WP | Distributed uniform load | Bottom Flange | Fixed | Prevented | 8.45 | 1213.20 | --- | --- | 502.29 | 1397.20 |

Table 4: Comparison of critical moments predicted by the developed FE model and those calculated by different analytical and numerical methods (relative values)

| ID | Loading | Point of load application | Support of both ends | Warping | FEM | AISC | SSRC | NR | LTBeam |
|---|---|---|---|---|---|---|---|---|---|
| DL-PS-TF-WF | Distributed uniform load | Top Flange | Pinned | Free | 1.00 | 0.85 | 1.04 | 1.04 | 1.02 |
| PL-PS-TF-WF | Concentrated force at midspan | Top Flange | Pinned | Free | 1.00 | 0.88 | 1.02 | 1.04 | 1.02 |
| EM-PS-MH-WF | Opposite and equal end moments | Midheight | Pinned | Free | 1.00 | 0.98 | 0.98 | 0.98 | 0.98 |
| DL-PS-MH-WF | Distributed uniform load | Midheight | Pinned | Free | 1.00 | 1.02 | 1.02 | 1.01 | 1.01 |
| PL-PS-MH-WF | Concentrated force at midspan | Midheight | Pinned | Free | 1.00 | 1.02 | 1.02 | 1.04 | 1.05 |
| DL-PS-BF-WF | Distributed uniform load | Bottom Flange | Pinned | Free | 1.00 | --- | 1.02 | 1.02 | 1.03 |
| PL-PS-BF-WF | Concentrated force at midspan | Bottom Flange | Pinned | Free | 1.00 | --- | 0.98 | 1.01 | 1.03 |
| PL-FS-TF-WF | Concentrated force at midspan | Top Flange | Fixed | Free | 1.00 | 1.41 | 1.64 | 1.54 | 0.88 |
| DL-FS-TF-WF | Distributed uniform load | Top Flange | Fixed | Free | 1.00 | 1.30 | 1.59 | 1.03 | 0.93 |
| PL-FS-MH-WF | Concentrated force at midspan | Midheight | Fixed | Free | 1.00 | 1.20 | 1.20 | 1.37 | 1.07 |
| DL-FS-MH-WF | Distributed uniform load | Midheight | Fixed | Free | 1.00 | 0.97 | 0.97 | 0.75 | 1.06 |
| PL-FS-BF-WF | Concentrated force at midspan | Bottom Flange | Fixed | Free | 1.00 | --- | 0.75 | 1.03 | 1.08 |
| DL-FS-BF-WF | Distributed uniform load | Bottom Flange | Fixed | Free | 1.00 | --- | 0.60 | 0.58 | 1.26 |
| PL-FS-TF-WP | Concentrated force at midspan | Top Flange | Fixed | Prevented | 1.00 | --- | --- | 1.53 | 1.07 |
| PL-FS-MH-WP | Concentrated force at midspan | Midheight | Fixed | Prevented | 1.00 | --- | --- | 1.32 | 1.31 |
| DL-FS-TF-WP | Distributed uniform load | Top Flange | Fixed | Prevented | 1.00 | --- | --- | 0.92 | 1.08 |
| DL-FS-MH-WP | Distributed uniform load | Midheight | Fixed | Prevented | 1.00 | --- | --- | 0.61 | 1.11 |
| PL-FS-BF-WP | Concentrated force at midspan | Bottom Flange | Fixed | Prevented | 1.00 | --- | --- | 0.83 | 1.14 |
| DL-FS-BF-WP | Distributed uniform load | Bottom Flange | Fixed | Prevented | 1.00 | --- | --- | 0.41 | 1.15 |

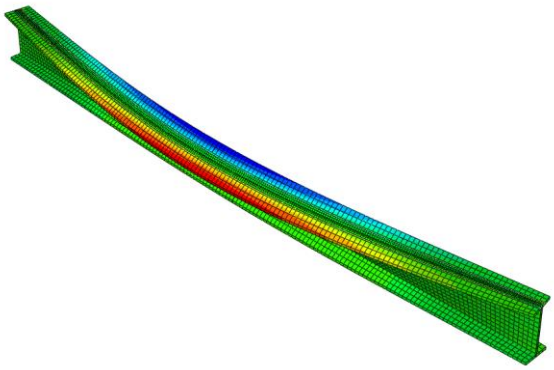

(a) warping-free pinned ends

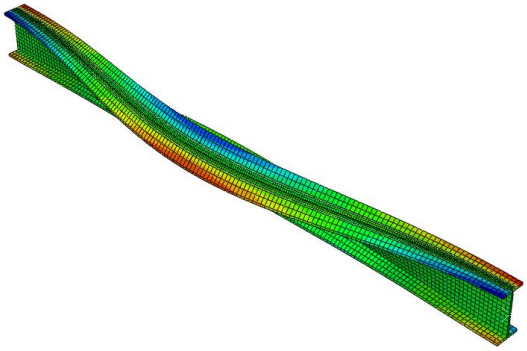

(b) warping-prevented fixed ends

Figure 4: FE critical mode shapes for distributed load applied at the top flange of a beam with fork supports (linear buckling analysis)

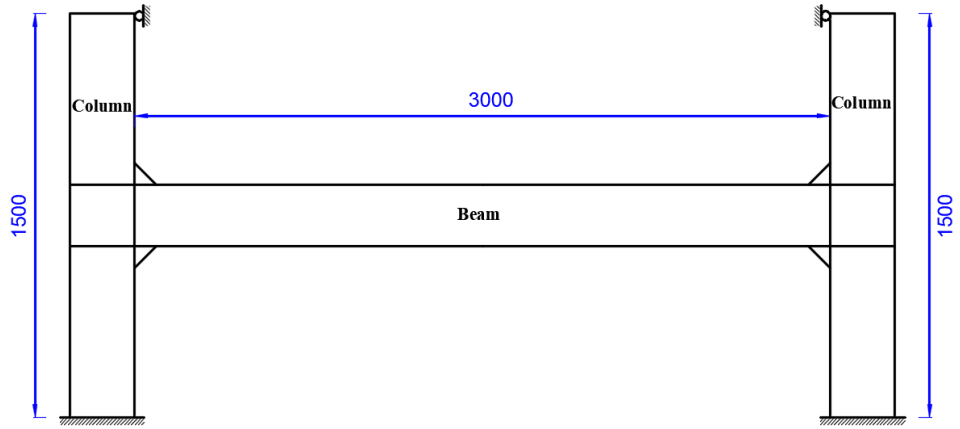


Figure 5: Schematic outline of beams connected to columns by end-plate joints (all dimensions are in mm)

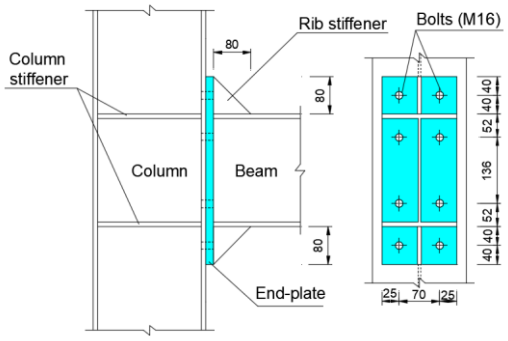


(a) stiffened extended end-plate

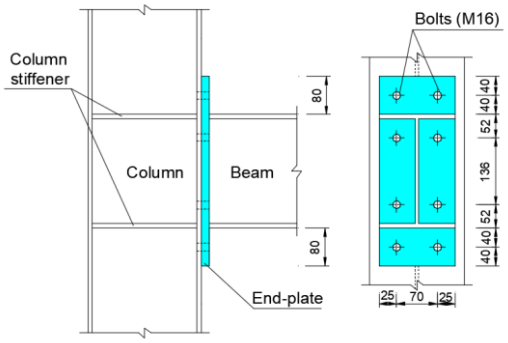


(b) unstiffened extended end-plate

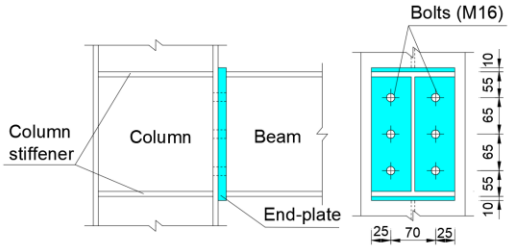


(c) flush end-plate

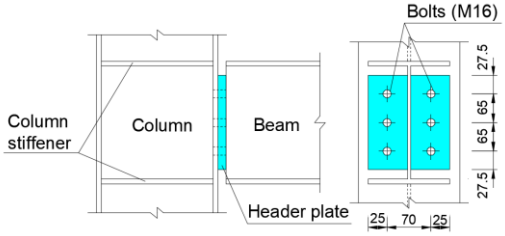


(d) shear end-plate

Figure 6: Details of the four connection configurations considered in the parametric study (all dimensions are in mm)

Two groups of beams connected to columns through end-plate connections were considered in the parametric study. In the first group, the outer depth; flange width; flange thickness; and web thickness of columns and beam were, respectively, 240, 120; 12; and 10 mm. This implies that the column-to-beam stiffness ratio of *Group I* equals unity. On the other hand, to study the effect of

column-to-beam stiffness ratio on the stability of frame beams, stiffer columns, with stiffness of 150% of beam stiffness, were employed in *Group II*.

## 5. Results and discussion

Table 5 compares the critical moments of beams with different end conditions (including fixed/pinned warping-free/warping prevented fork supports and four beam-to-column joint configurations), while the numerically-predicted critical mode shapes for distributed load imposed at the top flange of a beam joined to columns using different connection types. From the table, among the studied beam-to-column connection configurations, beams with stiffened extended end-plate (SEEP) joints had the highest critical moment (184 kN.m), whereas those with shear end-plate connections recorded the lowest critical moment (50% of that of SEEP connections).

Table 5: Critical moments of beams with different end conditions

| Conditions of both ends | $M_{cr}$ (kN.m) | $C_c$ |
|---|---|---|
| Shear end-plate (nominally pinned) beam-to-column joints | 93.56 | -0.10 |
| Fork supports - Pinned - Warping Free | 116.14 | 0.00 |
| Fork supports - Fixed - Warping Free | 159.55 | 0.20 |
| Flush end-plate beam-to-column joints | 162.36 | 0.21 |
| Unstiffened Extended end-plate beam-to-column joints | 165.92 | 0.23 |
| Stiffened Extended end-plate beam-to-column joints | 183.95 | 0.31 |
| Fixed - Warping Prevented | 333.33 | 1.00 |

As expected, the critical moments of beams with semi-rigid connection types (i.e. flush and extended end-plate connections) lie between the $M_{cr}$ of the beam with warping-free pinned fork supports and that of the beam with warping-prevented fixed supports. In terms of $M_{cr}$, the beam with shear end-plate joints is less than that of the beam with warping-free pinned fork supports. This surprising result can be attributed to the fact that the translational displacements in the cross-section plane are prevented in fork supports, but they are completely free in the case of shear end-plate connections (Fig. 8). This diminishes the critical buckling resistance of beams with shear end-plate joints and reaffirms the assumptions inherent in classical solutions for $M_{cr}$.

To account for end connection stiffness, a modification factor, $C_c$, is proposed. This factor determines how the critical moment of a beam is compared to both $M_{cr}$ of the same beam with warping-free pinned fork supports and $M_{cr}$ in the case of warping-prevented fixed ends. This modification factor can be calculated using the following equation:

$$M_{cr} = M_{crss} + C_c\left(M_{crfix} - M_{crss}\right) \quad (8)$$

where $M_{cr}$ is the critical moment of the considered beam, $M_{crss}$ is the critical moment of a beam with geometric and material properties, and loading conditions identical to the considered beam but with warping-free pinned fork ends, and $M_{crfix}$ is the critical moment of a beam with geometric and material properties, and loading conditions identical to the considered beam but with warping-prevented fixed ends.

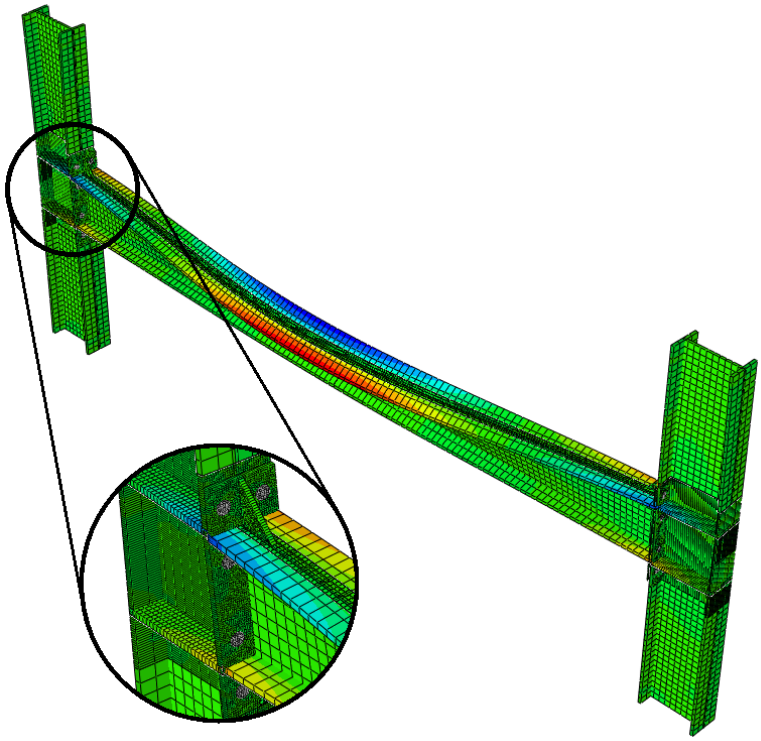

(a) stiffened extended end-plate

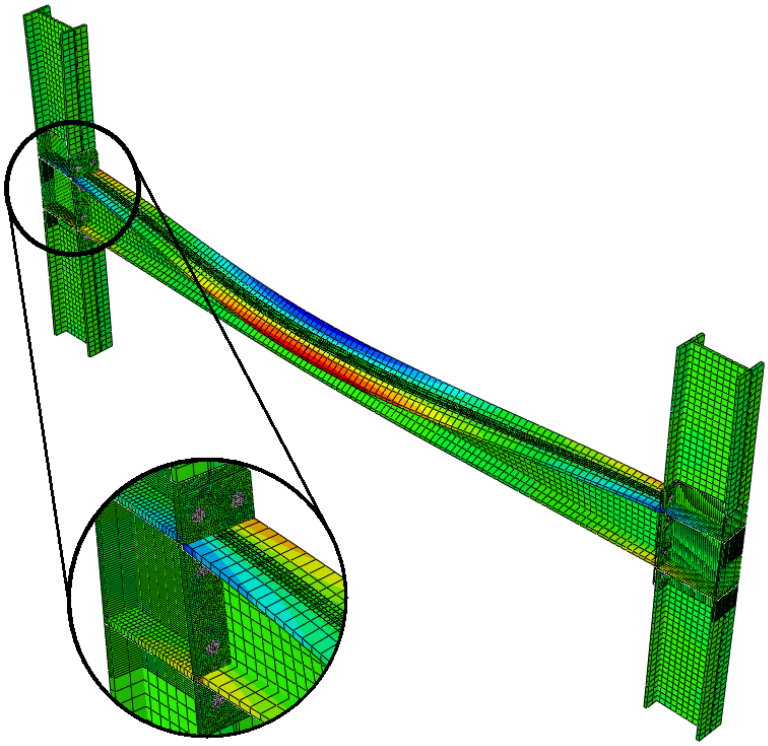

(b) unstiffened extended end-plate

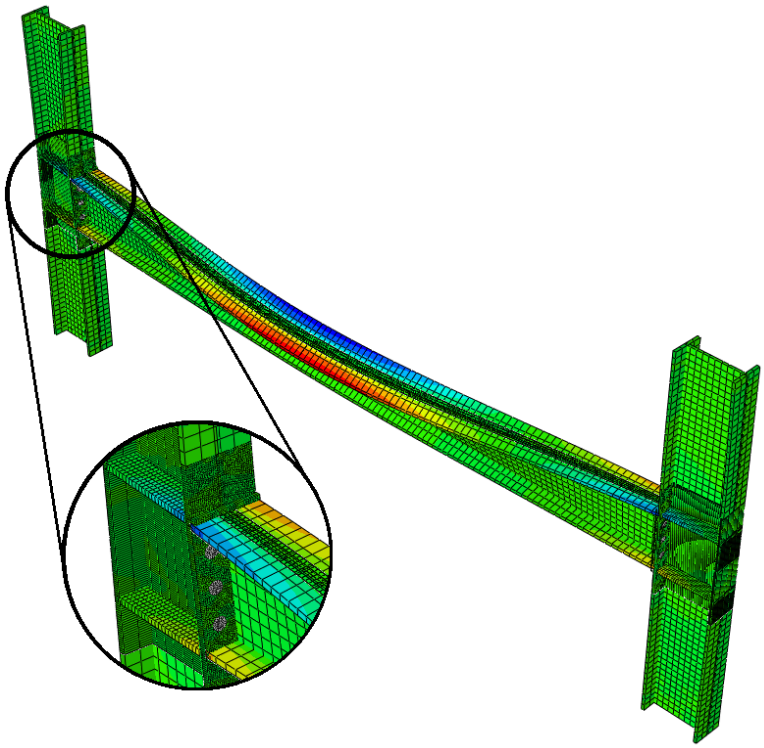

(c) flush end-plate

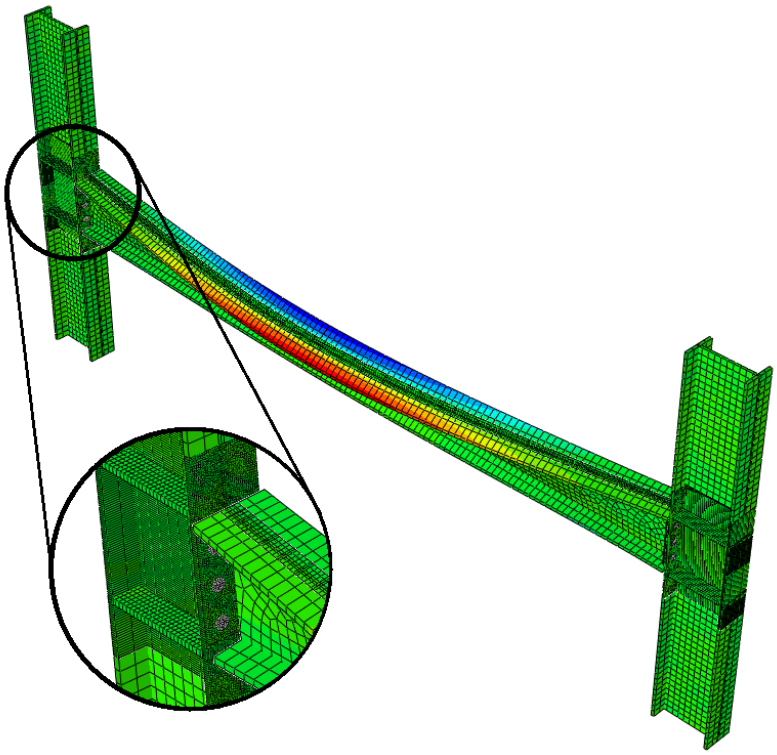

(d) shear end-plate

Figure 7: FE deformed shapes at the critical load for beams connected to two columns using different connection configurations (linear buckling analysis)

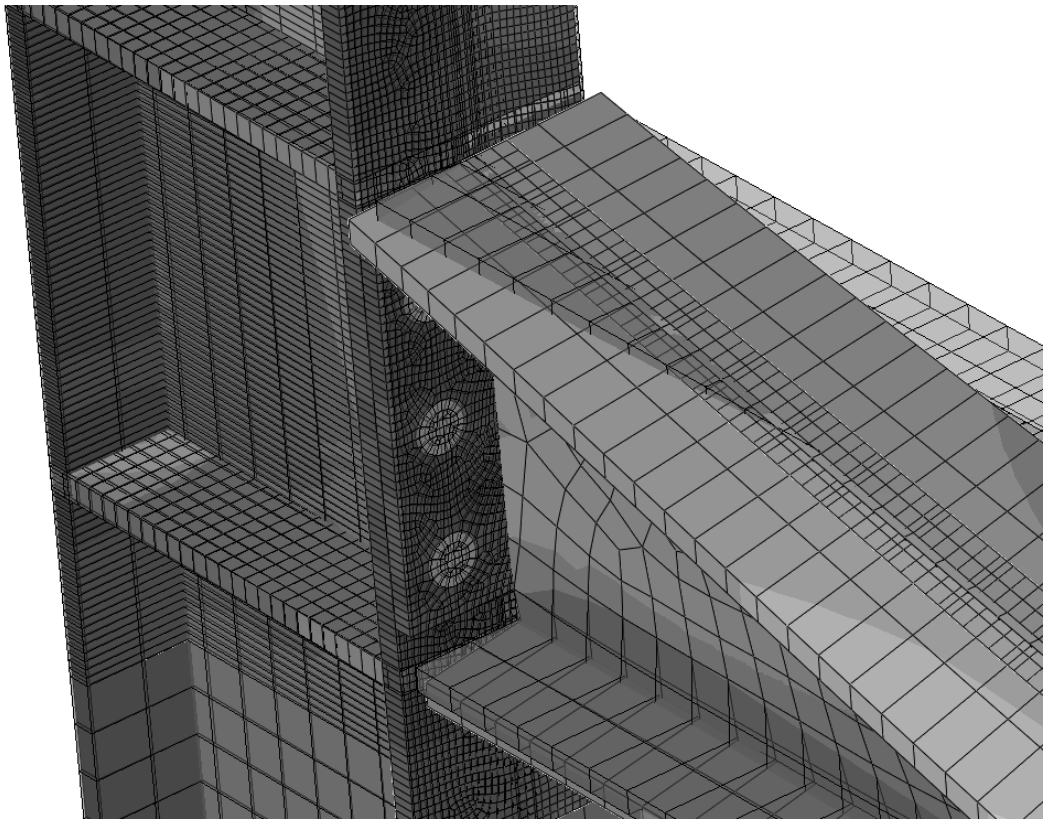

Figure 8: Deformed vs undeformed shapes of a beam connected to columns using shear end-plate connections

The values of the proposed modification factor $C_c$ are calculated for the beams investigated in the current parametric study and listed in Table 5. As expected from Eq. 8, $C_c$ is negative for beams with $M_{cr}$ less than $M_{crss}$ as in the case of shear end-plate connections, and positive (between 0 and 1) for beams whose critical moment is greater than $M_{crss}$, but less than $M_{crfix}$, as in the cases of flush and extended end-plate connections.

Table 6 presents a comparison between the critical moments of two groups of beams. Models in Group I have a column-to-beam stiffness ratio of 1, while the column-to-beam stiffness ratio in the second group equals 1.5. From the comparison, in the cases of semi-rigid connections (flush and extended-end plate connections), an increase in column-to-beam stiffness ratio (from 1 to 1.5) led to a corresponding increase in the critical moment of around 18%, and in turn a rise in $C_c$ values. On the other hand, increasing column-to-beam stiffness ratio has not resulted in any noticeable difference in $M_{cr}$ in the case of shear end-plate connections. This is not surprising because the main reason for the relatively low $M_{cr}$ of beams connected to columns by shear end-plates joints is the non-restrained translational displacements in the cross-section plane at beam ends. Employing stiffer columns has no impact on these free translational displacements (Fig. 8), and hence the critical moment of such beams remains almost unchanged.

Based on the above discussion, there could be a benefit to an extensive study aiming to investigate the linear and nonlinear lateral torsional buckling behavior of stainless steel beams with various

end conditions. Such a study can help in providing a better understanding of the effect of beam-to-column connection type on the stability of stainless steel frame beams, and its results can be exploited for developing an analytical method to calculate the modification factor proposed herein to account for end connection stiffness.

Table 6: Effect of column-to-beam relative stiffness on critical moment

| Conditions of both ends | $M_{cr}$ (kN.m) | | $C_c$ | |
|---|---|---|---|---|
| | Group I | Group II | Group I | Group II |
| Shear end-plate joints | 93.56 | 91.85 | -0.10 | -0.11 |
| Flush end-plate joints | 162.36 | 194.47 | 0.21 | 0.36 |
| Unstiffened Extended end-plate joints | 165.92 | 196.65 | 0.23 | 0.37 |
| Stiffened Extended end-plate joints | 183.95 | 213.93 | 0.31 | 0.45 |

## 6. Conclusions

A 3D shell FE model was developed to study the linear lateral torsional buckling (LTB) behavior of stainless steel beams with various end conditions. The shell FE model demonstrated the limitation of commonly available analytical methods for predicting the LTB buckling moment of beams, particularly when end rigidity and load height effects are both present. The stability of frame beams connected to columns through different types of end-plate connections was also investigated. Four connection configurations were considered in the study, including stiffened extended end-plate; unstiffened extended end-plate; flush end-plate; and shear end-plate connections. The results demonstrated that among the investigated beam-to-column connection types, a beam with stiffened extended end-plate connections had a critical moment of 184 kN.m, but for the same beam with shear end-plate joints the critical moment dropped to 93.6kN.m due to the unrestrained translational displacements in the cross-section plane at beam ends. This buckling moment is even lower than that of a beam with warping-free pinned fork supports. To account for end connection stiffness, a modification factor providing the degree to which the critical moment varies between its simply supported and fixed solution was proposed and calculated for the investigated beams, while its value was negative for shear end-plate connections it ranged from 0.21 to 0.45 for the studied semi-rigid connections. In terms of using stiffer columns, in the cases of flush and extended end-plate connections, an increase in column-to-beam stiffness ratio led to a corresponding increase in the critical moment. On the other hand, for shear end-plate joints, there was no noticeable difference in $M_{cr}$ due to employing stiffer columns. The study's findings highlight the need for performing further investigations into the linear and nonlinear lateral-torsional buckling performance of stainless steel frame beams with different beam-to-column connection types. The outcomes of such studies can be beneficial for the assessment of new design provisions for stainless steel structures.

## References

AISC. 2010a. Specification for structural steel buildings. ANSI/AISC standard 360-10. American Institution of Steel Construction, Chicago, IL.

AISC. 2010b. Commentary on the specification for structural steel buildings. American Institution of Steel Construction, Chicago, IL.

Anwar-Us-Saadat, M., & Ashraf, M. (2018). The continuous strength method for lateral-torsional buckling of stainless steel I-beams. *Thin-Walled Structures*, *130*, 148-160.

Baddoo, N. R. (2008). Stainless steel in construction: A review of research, applications, challenges and opportunities. *Journal of constructional steel research*, *64*(11), 1199-1206.

Bailey, C. G., Burgess, I. W., & Plank, R. J. (1996). The lateral-torsional buckling of unrestrained steel beams in fire. *Journal of Constructional Steel Research*, *36*(2), 101-119.

Bathe, K.J. (1998). Finite element procedures. New Jersey, Prentice-Hall.

Di Sarno, L., Elnashai, A. S., & Nethercot, D. A. (2003). Seismic performance assessment of stainless steel frames. *Journal of Constructional Steel Research*, *59*(10), 1289-1319.

Di Sarno, L., Elnashai, A. S., & Nethercot, D. A. (2006). Seismic retrofitting of framed structures with stainless steel. *Journal of Constructional Steel Research*, *62*(1-2), 93-104.

Eladly, M. M. (2020a). Behaviour of stainless steel beam-to-column bolted connections–Part 1: Simplified FE model. *Journal of Constructional Steel Research*, *164*, 105784.

Eladly, M. M. (2020b). Analytical study of unstiffened extended end-plate connections produced from austenitic stainless steel.

Fortan, M., & Rossi, B. (2021). Lateral Torsional Buckling of Welded Stainless Steel I-Profile Beams: Experimental Study. *Journal of Structural Engineering*, *147*(3), 04020342.

Galéa Y. (2003) Moment critique de déversement élastique de poutre fléchies-Présentation du logiciel LTBEAM - Revue Construction Métallique -2003–CTICM.

Gardner, L. (2005). The use of stainless steel in structures. *Progress in Structural Engineering and Materials*, *7*(2), 45-55.

Gedge, G. (2008). Structural uses of stainless steel—buildings and civil engineering. *Journal of constructional steel research*, *64*(11), 1194-1198.

Kala, Z. (2015). Sensitivity and reliability analyses of lateral-torsional buckling resistance of steel beams. *Archives of Civil and Mechanical Engineering*, *15*(4), 1098-1107.

Kucukler, M., Gardner, L., & Macorini, L. (2015). Lateral–torsional buckling assessment of steel beams through a stiffness reduction method. *Journal of Constructional Steel Research*, *109*, 87-100.

Nethercot, D.A., and Rockey, K.C. (1972). A unified approach to the elastic lateral buckling of beams. *Engineering Journal, 9(1)*, 96-107.

Real, P. V., Lopes, N., da Silva, L. S., & Franssen, J. M. (2008). Lateral–torsional buckling of stainless steel I-beams in case of fire. *Journal of Constructional Steel Research*, *64*(11), 1302-1309.

Real, P. V., Piloto, P. A. G., & Franssen, J. M. (2003). A new proposal of a simple model for the lateral-torsional buckling of unrestrained steel I-beams in case of fire: experimental and numerical validation. *Journal of Constructional Steel Research*, *59*(2), 179-199.

Rossi, B. (2014). Discussion on the use of stainless steel in constructions in view of sustainability. *Thin-Walled Structures*, *83*, 182-189.

Šorf, M., & Jandera, M. (2020, December). Lateral-torsional buckling of slender cross-section stainless steel beams. *Structures*, *28*, 1466-1478.

Wong, E., Driver, R. G., & Heal, T. W. (2015). Simplified approach to estimating the elastic lateral–torsional buckling capacity of steel beams with top-flange loading. *Canadian Journal of Civil Engineering*, *42*(2), 130-138.

Zhou, F., & Li, L. (2016). Experimental study on hysteretic behavior of structural stainless steels under cyclic loading. *Journal of Constructional Steel Research*, *122*, 94-109.

Ziemian, R. D. (Ed.). (2010). *Guide to stability design criteria for metal structures*. John Wiley & Sons.